Evaluating the Spatial Compliance of Circularly Curved-Beam Flexures

Farid Parvari Rad, Giovanni Berselli, Rocco Vertechy, and Vincenzo Parenti Castelli

Abstract In this paper, the closed-form compliance equations for Circularly Curved-Beam Flexures are derived. Following a general modeling procedure previously described in the literature, each element of the spatial compliance matrix is analytically computed as a function of both hinge dimensions and employed material. The theoretical model is then validated by comparing analytical data with the results obtained through Finite Element Analysis. Finally, a case study is presented concerning the potential application of these types of flexures in the optimal design of compliant robotic fingers.

Key words: Circularly Curved-Beam Flexures, compliance matrix, robotic fingers, Finite Element Analysis.

1 Introduction

A flexure hinge is a flexible connector that can provide a limited rotational motion between two parts by means of material deformation. According to [2], these connectors can be used to substitute traditional kinematic pairs (like bearing couplings) in rigid-body mechanisms, thus obtaining the so-called Lumped Compliant Mechanisms (LCMs), in which compliance is concentrated in relatively small regions connected through rigid links. When compared to their rigid-body counterpart, LCMs are characterized by reduced weight, absence of backlash and friction, part-count

Farid Parvari Rad, Vincenzo Parenti Castelli
Dept. of Mech. Eng., University of Bologna, Italy, e-mail: farid.parvarirad2@unibo.it, vincenzo.parenti@unibo.it
Giovanni Berselli
Dept. of Mech. Eng., University of Modena and Reggio Emilia, Italy e-mail: giovanni.berselli@unimore.it
Rocco Vertechy
Percro Lab., Scuola Superiore Sant'Anna, Italy, e-mail: r.vertechy@sssup.it

reduction, but restricted range of motion.

From a design perspective, the introduction of flexure hinges in serial articulated chains, like anthropomorphic hands and prosthesis, seems promising as it can allow the generation of very slender and light mechanisms that better reproduce biological structures. For instance, Fig. 1 and Fig. 2 depict two compliant robotic fingers, previously proposed by Lotti and Vassura [8], that employ either Straight-Beam Flexures (SBF) or Circularly Curved-Beam Flexures (CCBF) as possible substitutes for traditional revolute joints (the corresponding hinge rotation being defined as principal rotation [3]). In this case, regardless of the flexure topology, the use of flexible joints allows one-piece manufacturing and enhanced performance in terms of robustness and safety when interacting with unknown environments or humans (e.g. [4]). Despite the aforementioned advantages, LCMs also introduce new engineering challenges mainly due to possible fatigue failures and undesired spatial motions, which may occur under the action of out-of-plane forces also in LMCs initially conceived as planar mechanisms.

In this scenario, relatively simple models, such as the well-known pseudo-rigid-body model described in [5], can turn very useful for model-based control of robotic systems [1], and for designing LCMs with prescribed load-displacement profiles at one point on their structure [9]. In parallel, the knowledge of the hinge compliance behavior in the 3D space, even in the small displacement range where a 6x6 spatial compliance matrix can be defined, may become extremely valuable for both first attempt sizing the hinge dimensions and for comparison purposes. For instance, a method for comparing the selective compliance of elastic joints with generic morphology has been proposed in [3]. Empirical equations based on Finite Element Analysis (FEA) for various hinge profiles have been reported in e.g. [12], whereas the stiffness matrices concerning several hinge geometries (e.g. circular and elliptical) can be found in [7]. Furthermore, several studies concerned the stiffness analysis of curved beams by means of the Castigliano second theorem [10] or the so-called direct methods [6].

Following a similar approach, the contributions of this paper are: a) to report the closed-form compliance equations for CCBF (i.e. a particular case of generic curved beams); b) to compare CCBF and SBF in terms of selective compliance and maxi-

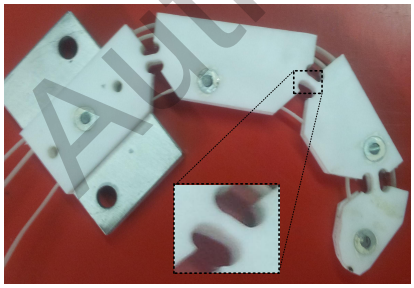

Fig. 1 Mono-piece robotic finger employing Straight-Beam Flexures [8]

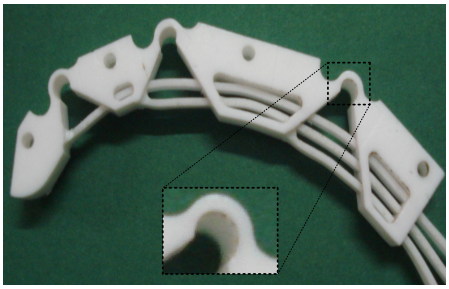

Fig. 2 Mono-piece robotic finger employing Circularly Curved-Beam Flexures [8]

mum achievable principal rotation. In particular, the CCBF and SBF employed for the fabrication of the robotic fingers depicted in Fig. 1 and Fig. 2 are considered as a case study, whereas the theoretical CCBF model is derived following the general procedure outlined in [6] and subsequently validated via FEA.

2 Closed-Form Compliance Equations

As previously said, the direct analytical method proposed in [6] is used for defining the CCBF flexural behavior. With reference to Fig. 3, let us consider a cantilever curved beam with a uniform cross section and generically loaded on the free end. Node 1 and node 2 are two points located on the beam fixed and free end respectively. The external load, **P**, and the corresponding deformation, **Q**, might be expressed in a predefined global coordinate system via the following column vectors:

$$\mathbf{P} = \begin{bmatrix} f_x & f_y & f_z & m_x & m_y & m_z \end{bmatrix}^{\mathbf{T}}; \qquad \mathbf{Q} = \begin{bmatrix} u & v & w & \alpha & \phi & \psi \end{bmatrix}^{\mathbf{T}} \tag{1}$$

where u, v, w and α, ϕ, ψ are, respectively, the three displacements of node 2 and the three rotations of the corresponding beam cross section along the x, y and z directions. With reference to Fig. 4, a local coordinate system centered on the centroid of a generic beam cross section can be defined. In particular, these local coordinates are denoted as **l**, **m** and **n**, namely the tangent vector and the principal vectors of the cross section [6]. The relation between local and global coordinates can be written as follows:

$$\begin{bmatrix} \mathbf{l} \\ \mathbf{m} \\ \mathbf{n} \end{bmatrix} = \begin{bmatrix} l_x(s) & l_y(s) & l_z(s) \\ m_x(s) & m_y(s) & m_z(s) \\ n_x(s) & n_y(s) & n_z(s) \end{bmatrix} \cdot \begin{bmatrix} \mathbf{i} \\ \mathbf{j} \\ \mathbf{k} \end{bmatrix} = \mathbf{R}(s) \cdot \begin{bmatrix} \mathbf{i} \\ \mathbf{j} \\ \mathbf{k} \end{bmatrix} \tag{2}$$

where s refers to the coordinate variable along the curve and $\mathbf{R}(s)$ is the rotation matrix that relates global and local coordinate frames. The curve defining the centroid of the beam cross sections, curve C, in the global coordinates can be expressed by:

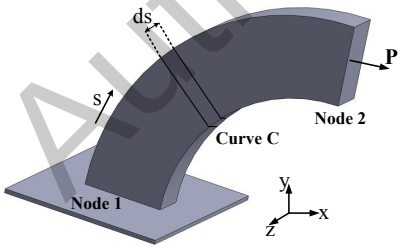

Fig. 3 Cantilever curved beam loaded at the free end

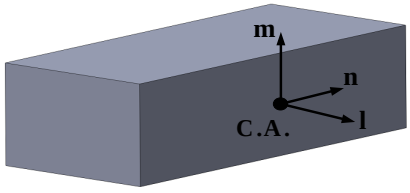

Fig. 4 Cross section of the beam and the local coordinates

$$\mathbf{r}(\mathbf{s}) = x(s)\mathbf{i} + y(s)\mathbf{j} + z(s)\mathbf{k} \tag{3}$$

The load $\mathbf{P}$ acting on the free end is balanced by a load $\mathbf{P}'$ acting on the element ds of the curve C. This load $\mathbf{P}'$ produces a deformation, $\mathbf{E}$, on the same element. The matrices $\mathbf{P}'$ and $\mathbf{E}$, together with the corresponding analytical relation can be expresses as:

$$\mathbf{P}' = \begin{bmatrix} f_l & f_m & f_n & m_l & m_m & m_n \end{bmatrix}^T; \quad \mathbf{E} = \begin{bmatrix} \varepsilon_{ll} & \gamma_{lm} & \gamma_{ln} & \kappa_{ll} & \kappa_{lm} & \kappa_{ln} \end{bmatrix}^T; \quad \mathbf{P}' = \mathbf{K} \cdot \mathbf{E} \tag{4}$$

The matrix $\mathbf{K}$ in Eq. 4 is the stiffness matrix of the element ds that can be written as:

$$\mathbf{K} = \begin{bmatrix} EA & 0 & 0 & 0 & 0 & 0 \\ 0 & \beta_m GA & 0 & 0 & 0 & 0 \\ 0 & 0 & \beta_n GA & 0 & 0 & 0 \\ 0 & 0 & 0 & GJ & 0 & 0 \\ 0 & 0 & 0 & 0 & EI_m & 0 \\ 0 & 0 & 0 & 0 & 0 & EI_n \end{bmatrix} \tag{5}$$

where A, β_m, β_n, I_m, I_n, J, E and G are, respectively, cross section area, shear coefficients, principal moments of inertia and polar moment of inertia of the beam's cross section, Young's modulus and shear modulus of the employed material. The deformation, $d\mathbf{Q}'$, of the element ds, due to the load $\mathbf{P}'$, is defined by:

$$d\mathbf{Q}' = \begin{bmatrix} du' & dv' & dw' & d\alpha' & d\phi' & d\psi' \end{bmatrix}^T = \mathbf{E} \cdot ds \tag{6}$$

where u', v', w' and α', ϕ', ψ' are respectively displacements and rotations of the element ds in the $\mathbf{l}$, $\mathbf{m}$ and $\mathbf{n}$ directions. The load $\mathbf{P}'$, acting on ds and due to the presence of a load $\mathbf{P}$ on the free end, can be computed via the adjoint transformation matrix $\mathbf{T} \in \mathbb{R}^{\mathbf{6}\times\mathbf{6}}$ between the global and local coordinates. The following relation holds:

$$\mathbf{P}' = \mathbf{T} \cdot \mathbf{P} \tag{7}$$

The adjoint matrix $\mathbf{T}$ is a function of s and can be computed from Eq. (2) and Eq. (3), as:

$$\mathbf{T} = \begin{bmatrix} \mathbf{R}^T & \mathbf{0} \\ (\widetilde{\mathbf{r}}_s \cdot \mathbf{R})^T & \mathbf{R}^T \end{bmatrix} \tag{8}$$

where $\mathbf{r_s} = \mathbf{r} - \mathbf{r_2}$ is the position vector connecting node 2 to the centroid of the section, $\mathbf{0} \in \mathbb{R}^{3\times3}$ is a null matrix, and $\widetilde{\mathbf{r}}_s$ denotes the cross product matrix of $\mathbf{r}_s$, i.e. the matrix such that $\widetilde{\mathbf{r}}\mathbf{u} = \mathbf{r} \times \mathbf{u}$ for any vector $\mathbf{u}$. In addition, the deformation of the element ds, $d\mathbf{Q}'$, causes a deformation at the free end, $d\mathbf{Q}$, that can be calculated using the following equation:

$$d\mathbf{Q} = \mathbf{T}^T \cdot d\mathbf{Q}' \tag{9}$$

By merging Eqs. (4), (6), (7) and (9), one obtains:

$$d\mathbf{Q} = \mathbf{T}^T \cdot \mathbf{K}^{-1} \cdot \mathbf{T} \cdot \mathbf{P} \cdot ds \tag{10}$$

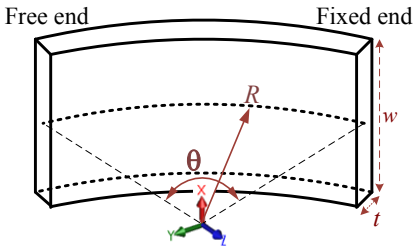

Fig. 5 Cross section properties and geometric parameters of the hinge

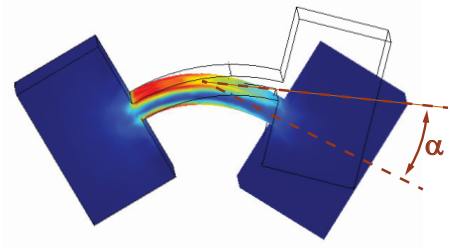

Fig. 6 FEA of the circularly curved-beam flexure hinge

By integrating Eq. (10), one can find the relation between the load, **P**, and the deformation, **Q**, of the free node, as follows:

$$\mathbf{Q} = \mathbf{C} \cdot \mathbf{P} \tag{11}$$

where:

$$\mathbf{C} = \int_C \mathbf{T}^T \cdot \mathbf{K}^{-1} \cdot \mathbf{T} \cdot ds \tag{12}$$

Matrix **C** is the compliance matrix for a general cantilever curved beam and it gives the relation between the loads at the free end and the corresponding deformations. This method is applied to a CCBF as the one depicted in Fig. 5, in order to estimate its compliant behavior under a generalized loading condition. Henceforth, the CCBF compliance matrix is derived in its analytical form and explicitly presented hereafter:

$$\mathbf{C} = \begin{bmatrix} C_{x,f_x} & 0 & 0 & 0 & C_{x,m_y} & C_{x,m_z} \\ 0 & C_{y,f_y} & C_{y,f_z} & C_{y,m_x} & 0 & 0 \\ 0 & C_{z,f_y} & C_{z,f_z} & C_{z,m_x} & 0 & 0 \\ 0 & C_{\theta_x,f_y} & C_{\theta_x,f_z} & C_{\theta_x,m_x} & 0 & 0 \\ C_{\theta_y,f_x} & 0 & 0 & 0 & C_{\theta_y,m_y} & C_{\theta_y,m_z} \\ C_{\theta_z,f_x} & 0 & 0 & 0 & C_{\theta_z,m_y} & C_{\theta_z,m_z} \end{bmatrix} \tag{13}$$

where:

$$C_{x,f_x} = R\left(\frac{\theta}{\beta_n GA} + \frac{R^2(3/2\,\theta - 2\sin(\theta) + 1/2\cos(\theta)\sin(\theta))}{GJ} + \frac{R^2(-1/2\cos(\theta)\sin(\theta) + 1/2\,\theta)}{EI_m}\right)$$

$$C_{x,m_y} = C_{\theta_y,f_x} = R\left(\frac{R(\sin(\theta) - 1/2\cos(\theta)\sin(\theta) - 1/2\,\theta)}{GJ} - \frac{R(-1/2\cos(\theta)\sin(\theta) + 1/2\,\theta)}{EI_m}\right)$$

$$C_{x,m_z} = C_{\theta_z,f_x} = R\left(-\frac{R\left(1/2\,(\cos(\theta))^2 - \cos(\theta)\right)}{GJ} + 1/2\,\frac{R(\cos(\theta))^2}{EI_m}\right)$$

$$C_{y,f_y} =$$

$$R\left(\frac{1/2\cos(\theta)\sin(\theta) + 1/2\,\theta}{EA} + \frac{-1/2\cos(\theta)\sin(\theta) + 1/2\,\theta}{\beta_m GA} + \frac{R^2(3/2\,\theta - 2\sin(\theta) + 1/2\cos(\theta)\sin(\theta))}{EI_n}\right)$$

$$C_{y,f_z} = C_{z,f_y} = R\left(1/2\,\frac{(\cos(\theta))^2}{EA} - 1/2\,\frac{(\cos(\theta))^2}{\beta_m GA} + \frac{R^2\left(1/2\,(\cos(\theta))^2 - \cos(\theta)\right)}{EI_n}\right)$$

$$\mathrm{C}_{y,m_x} = C_{\theta_x,f_y} = \frac{R^2(\theta-\sin(\theta))}{EI_n}$$

$$\mathrm{C}_{z,f_z} = R\left(\frac{-1/2\cos(\theta)\sin(\theta)+1/2\,\theta}{EA} + \frac{1/2\cos(\theta)\sin(\theta)+1/2\,\theta}{\beta_m GA} + \frac{R^2(-1/2\cos(\theta)\sin(\theta)+1/2\,\theta)}{EI_n}\right)$$

$$\mathrm{C}_{z,m_x} = C_{\theta_x,f_z} = -\frac{R^2\cos(\theta)}{Ei_n}$$

$$\mathrm{C}_{\theta_x,m_x} = \frac{R\theta}{EI_n}$$

$$\mathrm{C}_{\theta_y,m_y} = R\left(\frac{1/2\cos(\theta)\sin(\theta)+1/2\,\theta}{GJ} + \frac{-1/2\cos(\theta)\sin(\theta)+1/2\,\theta}{EI_m}\right)$$

$$\mathrm{C}_{\theta_y,m_z} = C_{\theta_z,m_y} = R\left(1/2\,\frac{(\cos(\theta))^2}{GJ} - 1/2\,\frac{(\cos(\theta))^2}{EI_m}\right)$$

$$\mathrm{C}_{\theta_z,m_z} = R\left(\frac{-1/2\cos(\theta)\sin(\theta)+1/2\,\theta}{GJ} + \frac{1/2\cos(\theta)\sin(\theta)+1/2\,\theta}{EI_m}\right)$$

$$\text{A=wt, } \mathrm{I}_m = 1/12\,tw^3, I_n = 1/12\,wt^3, J = I_m + I_n = 1/12\,wt\left(t^2+w^2\right)$$

In particular, with reference to Fig. 5, R, θ, w, t represent the radius of the hinge centroid with respect to the global coordinates, the angle of the centroid from the free to the fixed end, the hinge width and thickness respectively.

3 Numerical Example and Model Validation

As a case study, the compliant behavior of the CCBF and of the SBF depicted in Fig. 1 and Fig. 2 are numerically evaluated. As for the CCBF, the following geometric parameters are considered, namely $R = 30mm, t = 1.2mm, w = 6mm$ and $\theta = \pi/4$. The flexure hinge connects two rigid links located at a distance $l = 2R\sin(\theta/2)$ and is made of Acrylic Plastic with Young's modulus $E = 3000Mpa$, Poisson's ratio $\nu = 0.33$, shear modulus $G = 1130Mpa$ and the shear deformations being neglected. The principal hinge compliance [3] for the considered application is $C_{\theta_x,m_x} = 12R\theta/Ewt^3 = 9rad/Nm$. The method described in Sec. 2 is used for computing the overall CCBF compliance matrix, whereas Finite Element Analysis (FEA) is performed in order to validate the theoretical model. Figure 6 depicts, as an example, the CCBF undeformed and deformed shapes when subject to a flexural moment applied on the hinge free end. Similar FEA simulations are carried out by individually loading the CCBF at the free end for each component of the load **P** (that is individual forces and moments are applied) and obtaining the corresponding deformations (displacements and rotations). The ratio between each load and deformation component simply represents the compliance factors along different axes. The overall numerical results are shown in Tab. 1, which also depicts the percentage error between analytical and FEA methods. A maximum percentage error of less than 3% confirms the validity of the proposed modeling technique.

The same procedure is then applied to compute the SBF compliance matrix whose analytical solution is known from the literature [11]. As said, the SBF is designed so as to connect the same rigid links of the previous example and to provide the same principal compliance as the CCBF previously modeled. Henceforth, the SBF length

Table 1 Compliance factors for the CCBF flexure hinge and comparison between analytical and FEA results

Compliance factors	C_{x,f_x}	$C_{x,m_y} = C_{\theta_y,f_x}$	$C_{x,m_z} = C_{\theta_z,f_x}$	C_{y,f_y}	$C_{y,f_z} = C_{z,f_y}$	C_{θ_x,m_x}
Analytic	8.001e-5	3.016e-4	-5e-3	1.466e-4	4.483e-4	9.0903
FEA	7.746e-5	3.015e-4	-4.99e-3	1.457e-4	4.457e-4	9.0897
Percentage error	3.3	4.7e-2	6e-2	5.9e-1	5.8e-1	4.9e-4
Compliance factors	C_{z,f_z}	$C_{z,m_x} = C_{\theta_x,f_z}$	$C_{y,m_x} = C_{\theta_x,f_y}$	C_{θ_y,m_y}	$C_{\theta_y,m_z} = C_{\theta_z,m_y}$	C_{θ_z,m_z}
Analytic	1.5e-3	1.017e-1	2.72e-2	8.256e-1	-1.797e-1	4.662e-1
FEA	1.486e-3	1.017e-1	2.72e-2	8.271e-1	-1.803e-1	4.664e-1
Percentage error	3.4e-1	0	0	1.8e-1	3.2e-1	4.5e-2

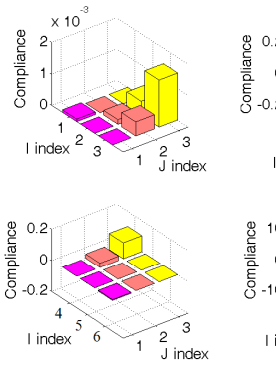

Fig. 7 3D bar representation for the compliance matrix of the CCBF

Fig. 8 3D bar representation for the compliance matrix of the SBF

is $l = 2R\sin(\theta/2)$, the SBF principal compliance is $\overline{C}_{\theta_x,m_x} = 12l/E\overline{w}\overline{t}^3 = 9rad/Nm$, whereas the SBF thickness, $\bar{t}$, is chosen accordingly as $\bar{t} = t\left(2\sin(\theta/2)/\theta\right)^{1/3}$. The numerical values of the compliance matrix entries are depicted in Fig. 7 and Fig. 8 respectively. Similarly to [3], this 3D bar graph representation allows a qualitative comparison of the hinge behavior in terms of selective compliance. It can be noticed that, in this particular case, the two solutions behave similarly. However, CCBF outperforms SBF in terms of maximum achievable principal rotation. In fact, these maximum rotations might be respectively computed as $\alpha_{CCBF} = max(\alpha_1, \alpha_2)$ and $\alpha_{SBF} = 2lS_Y/\bar{t}E$, the term S_Y being the material yield strength [11] and the terms α_1 and α_2 being defined in Eq. 14, such that $\alpha_{CCBF}/\alpha_{SBF} > 1$.

$$\alpha_1 = \frac{6R(t+R)S_y\theta\left(-2t+(t+2R)\mathrm{Log}\left[\frac{t+R}{R}\right]\right)}{t^2E\left(-t+(t+R)\mathrm{Log}\left[\frac{t+R}{R}\right]\right)}; \alpha_2 = 6E^{-1}RS_y\theta\left(\frac{t+2R}{t^2}+\frac{1}{-t+R\mathrm{Log}\left[\frac{t+R}{R}\right]}\right) \tag{14}$$

4 Conclusions

The closed-form compliance equations for CCBF have been presented and validated via FEA. A comparison has been carried out between CCBF and SBF for possible application in serial articulated chains, like robotic fingers. For this particular case, it is observed that the hinge compliance matrices are very similar, when comparing solutions having the same value of the principal compliance and connecting rigid links located at the same relative distance. Nonetheless, CCBF outperforms SBF in terms of maximum achievable principal rotation. Future work includes a detailed analysis of the CCBF properties as a function of the hinge geometrical parameters and an in-depth investigation of the hinge behavior in the large displacement range.

References

[1] Albu-Schäffer, A., Ott, C., Hirzinger, G.: A unified passivity-based control framework for position, torque and impedance control of flexible joint robots. The International Journal of Robotics Research **26**(1), 23–39 (2007)
[2] Ananthasuresh, G., Kota, S.: Designing compliant mechanisms. Mechanical Engineering **117**, 93–6 (1995)
[3] Berselli, G., Vassura, G., Piccinini, M.: Comparative evaluation of the selective compliance in elastic joints for robotic structures. IEEE ICRA, International Conference on Robotics and Automation pp. 759–764 (2011)
[4] Dollar, A., Howe, R.: A robust compliant grasper via shape deposition manufacturing. IEEE/ASME Transactions On Mechatronics **11**(2), 154–161 (2006)
[5] Howell, L.L.: Compliant mechanisms. Wiley, New York (2001)
[6] Jafari, M., Mahjoob, M.: An exact three-dimensional beam element with nonuniform cross section. ASME Journal of Applied Mechanics **77**(6) (2010)
[7] Lobontiu, N.: Compliant Mechanisms: Design of Flexure Hinges. CRC Press (2002)
[8] Lotti, F., Vassura, G.: A novel approach to mechanical design of articulated fingers for robotic hands. In: IEEE/RSJ IROS International Conference on Intelligent Robots and Systems (2002)
[9] Meng, Q., Berselli, G., Vertechy, R., Castelli, V.P.: An improved method for designing flexure-based nonlinear springs. ASME IDETC International Design Engineering Technical Conferences, Chicago, USA pp. 1–10 (2012)
[10] Palaninathan, R., Chandrasekharan, P.: Curved beam element stiffness matrix formulation. Computers & Structures **21**(4), 663–669 (1985)
[11] Timoshenko, S., Goodier, J.: Theory of Elasticity. 3. McGraw Hill Higher Education (1970)
[12] Yong, Y.K., Lu, T., Handley, D.: Review of circular flexure hinge design equations and derivation of empirical formulations. Precision Engineering **32**, 63–70 (2008)